THE ASIAN BULLETIN OF BIG DATA MANAGMENT
Vol. 5. Issue 1.1 (2025)
https://doi.org/10.62019/abbdm.v5i3.355

Localization and Detection of Cardiovascular Diseases using Artificial Intelligence

Sundus Baloch, Samra Hassan, Shabana Hajno, Saad Qasim, Ramsha Shuaib, Muhammad Mustafa

Chronicle

Article history
Received: May 2, 2025
Received in the revised format: May 27, 2025
Accepted: June 20, 2025
Available online: July 10, 2025

Sundus Baloch is currently affiliated with the Department of Computer Science, Fazaia Bilquis College of Education for Women's, PAF, Nur Khan Base, Rawalpindi, Air University, Islamabad, Pakistan.
Email: balochsundus18@gmail.com

Samra Hassan, Saad Qasim & Ramsha Shuaib are currently affiliated with the NUST Institute of Civil Engineering، School of Civil and Environmental Engineering، National University of Sciences and Technology, Pakistan.
Email: samrasarfaraz3@gmail.com
Email: Saadqasmkhan@gmail.com
Email: ramshaedu27@gmail.com

Shabana Hajno is currently affiliated with the Department of Computer Systems Engineering, Mehran University of Engineering and Technology, Jamshoro, Pakistan.
Email: hajanoshabana@gmail.com

Muhammad Mustafa is currently affiliated with the Health Services Academy, Islamabad Pakistan.
Email: Mustafasaqlain4@gmail.com

Corresponding Author*

Abstract

Cardiovascular diseases (CVDs) remain a leading global cause of death, with early diagnosis being critical to improving outcomes. Traditional electrocardiogram (ECG) analysis, especially in under-resourced settings like interior Sindh, Pakistan, often suffers from inaccuracies due to reliance on outdated, manual interpretation and limited-lead data. This research presents a smart diagnostic framework that leverages a hybrid Faster Region-based Convolutional Neural Networks (Faster-RCNNs) and Region Proposal Networks (RPN) for high-fidelity feature extraction and disease localization from 12-lead ECGs. Unlike existing models focused on 1- or 6-lead inputs, the proposed system processes full 12-lead data to segment waveform components (P, QRS, T waves), quantify intervals (PR, QT, RR), and detect abnormalities such as ST deviations and Corrected QT interval (QTc) prolongation. A key innovation of this work is the integration of Explainable AI (XAI) through a clinical rule-based inference engine—referred to as the Condition Combiner—which interprets extracted features using cardiology-derived expressions. This XAI layer emulates expert reasoning, providing transparent and clinically interpretable diagnoses. The system is capable of detecting and localizing over 55 cardiac conditions, including myocardial infarctions, arrhythmias, conduction blocks, and electrolyte imbalances. To the best of our knowledge, our model offers maximum possible heart related issues which amounts to 55 different cardiac diseases. The proposed system has the capability to localize heart disease as well, with decent accuracy. The model achieved a 91.2% Exact Match Accuracy and F1 scores 93% across all conditions, demonstrating strong generalization and clinical reliability. Designed with scalability in mind, the system offers an explainable, automated solution suitable for both hospital-grade deployments and low-infrastructure healthcare settings, advancing early detection of cardiac diseases with trust and interpretability.

Keywords: ECG, FASTER-RCNN, Cardiac disease detection, explainable AI, 12-lead, deep learning, disease localization.

INTRODUCTION

Cardiovascular diseases (CVDs) are among the primary causes of morbidity and mortality globally, accounting for nearly 18 million deaths annually (WHO, 2021). These diseases encompass a wide spectrum of conditions affecting the heart and blood vessels, including myocardial infarction, arrhythmias, heart failure, and ischemic diseases. Given the substantial burden these conditions impose on global health systems, there is an urgent need for effective, scalable, and precise diagnostic tools (Webster, 2010). One of the most widely used tools in cardiovascular diagnostics is the electrocardiogram (ECG), a non-invasive method that records the electrical activity

of the heart over time using surface electrodes (Kligfield et al., 2007). The 12-lead ECG, in particular, offers a comprehensive view of cardiac electrophysiology, enabling clinicians to assess and localize abnormalities with high spatial resolution. This modality captures electrical activity from multiple angles of the heart, providing critical insights into issues such as myocardial ischemia, infarction, bundle branch blocks, and hypertrophy (Deng et al., 2024), (Raun et al., 2019). Unlike 1-lead or 6-lead ECGs commonly used in mobile and wearable health technologies, the 12-lead format allows for regional diagnosis, crucial in managing complex cardiac conditions. Despite its diagnostic utility, interpreting a 12-lead ECG accurately requires significant expertise and training, which can be inconsistent across healthcare settings, especially in resource-constrained regions (Siam et al., 2024). Errors in interpretation can lead to misdiagnosis, delayed treatment, and increased mortality. Furthermore, the shortage of trained cardiologists in rural and underserved areas exacerbates these challenges. This necessitates the development of intelligent and automated ECG interpretation systems to bridge the diagnostic gap (MAbdou et al., 2024), (Wu et al., 2025).

Recent advancements in machine learning (ML) and deep learning (DL) have opened new avenues for automating ECG analysis (Martinez-Selles et al., 2023). CNNs and Recurrent Neural Networks (RNNs) have been widely adopted for tasks like arrhythmia detection, feature extraction, and rhythm classification (Hannun, A. Y. et al., 2024),(Raghunath et al., 2020). Transfer learning and ensemble methods have also been used to improve generalization and performance across different datasets (Basheer et al., 2024), (Hughes, J Weston et al., 2023). However, most studies use reduced-lead data due to ease of access and lower computational overhead. These configurations, while suitable for wearable monitoring, compromise the spatial resolution needed for accurate disease localization (Gui et al., 2024), (L. Zhao et al., 2024).

Moreover, reduced-lead models often lack the interpretability crucial for clinical acceptance. Clinicians need to understand the basis for AI-driven decisions to trust and integrate them into practice. This shortfall can be addressed by employing Faster-Region-based Convolutional Neural Networks (Faster-RCNNs), which offer a structured, interpretable approach to waveform segmentation and disease localization (Kirkbas, A .et al, 2025), (Saglietto, Andrea .et al, 2024). Faster-RCNNs, initially developed for object detection in images, have demonstrated remarkable capabilities in segmenting regions of interest in ECG waveforms, such as P-waves, QRS complexes, and T-waves. By computing critical time intervals (e.g., PR, QRS, QT) and analyzing waveform morphology, these systems can detect anomalies like ST elevation or T-wave inversion with lead-specific precision (Mason .et al, 2024),(P. Rajpurkar, Hannun .et al, 2019),(P. Rajpurkar, Hannun .et al, 2019). These features are particularly valuable for diagnosing myocardial infarction, hypertrophy, and conduction blocks (K. He .et al, 2016), (J. Deng .et al, 2009).

Several studies have highlighted the advantage of FASTER-RCNN-based systems when combined with domain-specific knowledge. For instance, integrating diagnostic rules from the American Heart Association and cardiology textbooks into the model's logic boosts both performance and interpretability (Reddy .et al, 2022), (Kalmady .et al, 2024). Furthermore, platforms such as PhysioNet provide extensive 12-lead ECG datasets that enable robust training and validation of such models (Alsekait .et al, 2024), (Mishra, Siddharth et al., 2021). Additionally, combining FASTER-RCNN output with rule-based diagnostic engines ensures both transparency and adherence to

clinical standards. This hybrid model enhances diagnostic reliability while offering logical reasoning, such as "ST elevation ≥ 1 mm in leads II, III, and aVF indicates inferior wall MI," echoing cardiologist interpretation (Jin, L., 2024; Abaidullah & Basheer, 2024; Baker, Peter O et al., 2025). It also allows for improved multi-label classification, crucial for patients presenting with co-morbid cardiac abnormalities (Baek, Yong-Soo et al., 2025).

Key Contributions of this Research:

- First integration of Faster-RCNNs with clinical rule-based inference (Condition Combiner) for ECG analysis
- Combines deep learning-based feature extraction with transparent, interpretable diagnostic logic
- Detects and localizes **55 cardiac conditions** - largest coverage in literature
- Processes scanned ECG images (not just digital signals)
- RPN-guided Faster-RCNN architecture for precise waveform segmentation
- Multi-task loss function: Binary Cross-Entropy + Smooth L1 Loss
- Lead-specific anomaly mapping to cardiac anatomy

LITERATURE REVIEW

The diagnosis of cardiovascular diseases (CVDs)which remain the foremost cause of global mortality—has long relied on electrocardiograms (ECGs) as a frontline diagnostic modality (WHO, 2021). Traditional ECG interpretation, however, depends heavily on the clinical expertise of human evaluators, introducing variability, subjectivity, and diagnostic inconsistencies, especially in under-resourced settings such as interior Sindh, Pakistan (MAbdou et al., 2024). In these regions, the shortage of trained personnel and limited access to advanced digital infrastructure further compound the challenge of timely and accurate diagnosis.

To mitigate these challenges, a growing body of research has turned to machine learning (ML) and deep learning (DL) techniques to automate and enhance ECG analysis. Within the deep learning landscape, Convolutional Neural Networks (CNNs) have emerged as a dominant architecture for ECG signal classification. Landmark models like the one developed by Rajpurkar et al. (Huo et al., 2024) have achieved cardiologist-level performance in arrhythmia detection using single-lead ECGs. Similarly, RNNs and hybrid CNN-RNN models have been employed to model temporal dependencies within ECG sequences (Lin, Ching- et al., 2025). However, despite their classification prowess, these architectures function largely as black-box systems, offering little in terms of interpretability or insight into how decisions are made—an essential requirement in clinical diagnostics.

A more recent evolution in the field involves the integration of attention mechanisms to improve interpretability. The DANet model (Lin, Ching- et al., 2025), for instance, uses disease-specific attention maps to highlight diagnostically relevant waveform segments, allowing clinicians to visualize the model's focus during classification. However, even with this enhancement, such models remain limited in scope, primarily targeting arrhythmias and failing to address a broader range of conditions such as MIs, electrolyte imbalances, and bundle branch blocks. In contrast, Region Proposal Network(RPN)+Faster-Region-based Convolutional Neural Networks (Faster-RCNNs) originally designed for object detection and segmentation in computer vision—offer a promising yet underexplored avenue for ECG analysis. As described by Kirkbas et al. (Li et al.,2024). Faster-RCNNs are capable of detecting spatially defined regions of

interest within visual data. Leveraging this strength, the present study adapts Faster-RCNNs for segmenting ECG waveforms to extract clinically significant features such as the P-wave, QRS complex, ST-segment, and T-wave, along with precise interval calculations (e.g., PR, QRS, QT, RR) and morphological abnormalities like ST elevation or T-wave inversion. These segmented features are subsequently fed into a rule-based diagnostic engine constructed from cardiology literature and clinical best practices.

Unlike conventional end-to-end deep learning models that generate opaque classifications, this hybrid Faster-RCNN-rule engine offers transparent, explainable diagnostics. For example, the system can explain a diagnosis of Lateral Wall MI through logical expressions such as "ST elevation ≥ 1 mm in I and aVL, poor R wave progression in V3, and biphasic T-waves in V1–V5"—criteria that closely mirror those used by cardiologists in manual diagnosis. This approach not only enhances clinical trust but also allows for direct integration into medical workflows. The RPN+FASTER-RCNN-based system developed in this study uniquely bridges these gaps by combining high-resolution feature extraction with a rule-based inference engine. It is capable of diagnosing over 55 distinct cardiac conditions with lead-specific localization, and its performance—validated by an Exact Match Accuracy of 91.2% and F1 scores exceeding 90% for all conditions—sets a new benchmark for interpretable, scalable, and clinically relevant ECG analysis.

A comparative analysis with contemporary models from 2023 to 2025 further highlights the unique advantages of this framework summarized below in table 1. The SEER model from Stanford (Yin et al., 2025), for example, predicted five-year cardiovascular mortality using CNNs on 12-lead ECGs but lacked disease-specific diagnostics and interpretability. ECG-MACE (Jin, L., 2024), another notable model, focused on predicting major adverse cardiac events using multitask learning but did not provide segmented waveform insights or multi-label disease classification (Qadiret al.,2024). Similarly, the Dual Deep Learning system proposed by Lopes et al. (Jin, L., 2024) digitized scanned ECGs and applied CNN-based classification, yet its inability to offer lead-specific localization or diagnostic logic limited its utility for real-time clinical decision-making.

Table 1.
Critical Analysis Table

Study / Model	Lead Configuration	Model Type	Feature Localization	Rule-Based Diagnosis	Interpretability	Disease Scope	Clinical Deployment Readiness	Comparative Accuracy
Current Research	Full 12-lead	RCNN + Rule Engine	Precise P-QRS-T detection with bounding boxes	Clinical expression-based engine	Transparent (rule + annotation)	55+diseases (MI, arrhythmias, blocks, electrolytes)	Rural-ready, scalable, interpretable	-
Dual DL System (Wu et al., 2025)	Full 12-lead	CNN + CV	None	None	Post hoc analysis only	Broad classes, unverified rules	Experimental digitization model (90%)	92%

ECG-MACE (L. Zhao et al., 2024)	Full 12-lead	Multitask DL	None	None	Basic AUROC interpretation	Cardiovascular events only	Early clinical trials (95%)	94%
DANet (Jin, L., 2024)	Variable (mainly 12-lead)	Attention DL	Attention heatmaps	None	Partial (visual attention)	Arrhythmias only	Academic proof-of-concept (92%)	96%
SEER (Hughes, 2023)	Full 12-lead	CNN	None	None	Black box	Mortality risk only	High-resource hospitals (93%)	95%

METHODOLOGY

Research flow methodology

The flowchart in figure 1 visually outlines the step-by-step process of ECG-based cardiac disease detection using a smart system. The process begins with the input of a 12-lead ECG image, which is then passed to the detection module that identifies the recording speed of the ECG, either 25 mm/s or 50 mm/s. This detection is crucial, as it affects the scaling of time and amplitude in subsequent analysis.

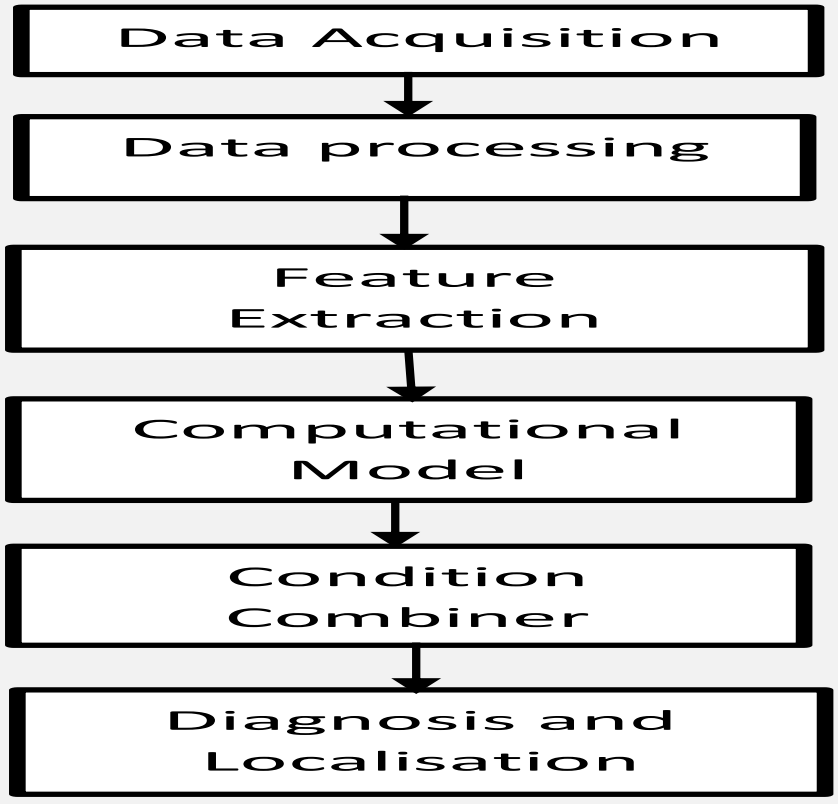

Figure1.
Research Flow Methodology

Once the speed is determined, the system proceeds to extract key waveform features such as P, QRS, and T intervals and populates these into a structured table according to the timing scale. These features are then forwarded to the calculation model, which generates expression-based outputs for each parameter by comparing them

to clinically accepted normal ranges. The generated expressions are processed through the condition combiner, a rule-based engine that assesses whether combinations of anomalies meet the diagnostic criteria for specific cardiac conditions. Finally, the system produces a diagnosis and localization output, identifying the type of heart disease present and its anatomical region within the heart. This streamlined, automated flow enables accurate, explainable, and scalable ECG interpretation.

A. Data Acquisition

The implementation of this study began with data acquisition, where 12-lead ECG images were collected from publicly available databases from the physionet library (https://doi.org/10.13026/bd2x-mf68) and clinical sources. These images underwent preprocessing steps, such as noise removal and contrast enhancement, to ensure clarity and facilitate accurate analysis. The core of the analysis relied on the application of Faster-Region-based Convolutional Neural Networks (Faster-RCNNs), which were used to segment ECG waveforms and detect key features including P-wave amplitude, PR interval, QRS duration, QRS axis, QT interval, ST-segment deviations, and T-wave amplitude and inversion. Following segmentation, pixel-based measurements were applied to convert grid spacing into clinically interpretable time intervals and amplitude values.

B. Data Processing

When processing ECGs recorded at a paper speed of 50 mm/s, it is essential to adjust the feature extraction algorithms to reflect the altered temporal resolution. At this speed, each small box on the ECG grid represents 20 milliseconds instead of the 40 milliseconds associated with the standard 25 mm/s setting, while each large box spans 100 milliseconds rather than 200. However, the vertical scaling for amplitude remains unchanged—10 millimeters still equal 1 millivolt, ensuring consistency in voltage interpretation. Next, these pixel distances are recalculated into meaningful time intervals using the 50 mm/s scale.

C. Feature extraction

To enhance the automated analysis of ECG signals, a Region-based Convolutional Neural Network (FASTER-RCNN) integrated with a Region Proposal Network (RPN) was implemented. The RPN serves as a precursor module that scans ECG waveforms using a sliding window mechanism to generate region proposals where significant cardiac features (e.g., P-wave, QRS complex, T-wave) are likely to appear. These proposals are passed to FASTER-RCNN, which applies convolutional layers to extract hierarchical features, followed by region-wise classification and bounding box regression. This two-stage architecture enables precise localization and labeling of key ECG components across 12 leads, facilitating the extraction of clinically relevant metrics such as RR intervals, ST-segment deviations, and QT intervals. The combined RPN-FASTER-RCNN approach ensures improved spatial resolution and diagnostic accuracy, particularly in complex ECG patterns associated with diverse cardiac pathologies.

D. Computation Model

The Calculation Model is a computational engine designed to transform raw ECG waveform measurements into clinically interpretable expressions. These expressions act as diagnostic signals—numerical representations of the conditions that underlie various cardiac pathologies.

One of the essential computations in ECG interpretation is the RR interval, calculated as the time difference between successive R-peaks, using the formula

$$RR_i = R_{i+1} - R_i \text{-----eq (1)}$$

The calculation of the RR interval—which measures the time between two successive R-peaks—is foundational for determining heart rate and assessing rhythm regularity. In eq 1, $R_i and\ R_{i+1}$ are the time points of two consecutive R-waves. Using this sequence of RR intervals, the system computes heart rate variability

Heart Rate Variability (HRV) features are derived from the RR intervals given in eq 1:

$$MeanRR(HRV) = \frac{1}{N}\sum_{i=1}^{N} RR_i \text{-----eq (2)}$$

Where N represents the total number of RR waveforms in one ECG graph For ST-segment analysis, deviations were assessed relative to the isoelectric baseline. The baseline voltage (V_{base}): was determined by averaging the voltage in the PR segment:

$$V_{base} = \frac{1}{N}\sum_{t=t_{start}}^{t_{end}} x(t) \text{------eq (3)}$$

Where N represents the total number of RR waveforms in one ECG graph, and x(t) is the voltage from a certain starting point to ending point.

Whereas $ST_{Deviation}$ measures the voltage deviation 60–80 milliseconds after the J-point:

$$ST_{Deviation} = x(t_{st}) - V_{base} \text{------eq (4)}$$

Where t_{st} is 60–80 ms after the QRS complex ends and $x(t_{st})$ is the voltage at that point.

For each lead ($x_i(t)$), computing features such as:

1. **P-wave Duration**: Duration between the start and end of the P-wave:

$$P_{duration} = t_{p_{end}} - t_{p_{start}} \text{------eq (5)}$$

Where $t_{p_{end}}$ is the end of p wave and $t_{p_{start}}$ is the start of p wave.

2. **QRS Duration**: Duration between the start and end of the QRS Complex:

$$QRS_{duration} = t_{QRS_{end}} - t_{QRS_{start}} \text{------eq (6)}$$

Where $t_{QRS_{end}}$ is the end of QRS wave and t_{QRS} is the start of QRS wave.

3. **QT Interval**: Duration between the start and end of the QT interval:

$$QT_{duration} = t_{T_{end}} - t_{QRS_{start}} \text{ ------eq (7)}$$

Where $t_{T_{end}}$ is the end of T wave and $t_{QRS_{start}}$ is the start of QRS wave.

4. **Amplitude**: Amplitudes of P, Q, R, S, and T waves are calculated as peak values relative to the isoelectric baseline.

To accommodate this temporal scaling, several key adjustments are integrated into the FASTER-RCNN-based feature extraction pipeline. First, the FASTER-RCNN is tasked with detecting and segmenting essential ECG waveform components, including the P-wave, PR interval, QRS complex, QT interval, ST segment, and T-wave amplitude.

These segments are isolated using bounding boxes, and the pixel distances between their respective boundaries are measured for further analysis.

Heart rate (HR) beats per minute (bpm) calculations are also adjusted accordingly. At 50 mm/s, the standard formula used is

$$HR(bpm) = \frac{3000}{Number\ of\ small\ boxes\ between\ R\ peaks.}$$ ------eq (8)

In contrast to the conventional 1500 divisor used at 25 mm/s. This recalibration ensures that heart rate estimations remain accurate despite the altered time scale.

Lastly, amplitude measurements—though unaffected by the paper speed—are computed by measuring the vertical pixel height of waveform components such as the P-wave, QRS complex, T-wave, and any ST-segment deviations. These pixel heights are then converted into millivolts using the equation:

$$Amplitude\ in\ mV\ = \frac{Pixel\ Height\ per\ mm}{Pixels} x\ 0.1$$ ------eq (9)

This formula in equation 3.7 assumes the standard calibration of 10 mm per millivolt. By incorporating all these modifications, the system ensures that ECGs recorded at 50 mm/s are analyzed with precision, consistency, and full clinical interpretability.

The ST-segment deviation (ΔST) is a critical metric used in ECG analysis to detect ischemic changes and myocardial infarction. It is measured 60 to 80 milliseconds after the J-point and is calculated relative to the isoelectric baseline, which is typically determined by averaging the voltage within the PR segment. Deviations above or below this baseline indicate abnormal repolarization patterns in the heart. In addition, the QRS complex duration (QRSd) is another fundamental parameter that reflects the time taken for ventricular depolarization. It is measured from the beginning to the end of the QRS complex and is essential for identifying conduction delays, such as bundle branch blocks or ventricular hypertrophy. Together, these features play a crucial role in the accurate diagnosis of various cardiac conditions.

This step generates a matrix of expressions per ECG lead. Each row corresponds to a feature (e.g., QTc), and each column to a lead (e.g., V1–V6), forming the mathematical groundwork for rule-based classification.

Table 2.
Amplitude differences between successive waves on ECG images

Wave	Amplitude Differences (mV)
P-P	[0.02, 0.01, 0.02, 0.01, 0.03, 0.01, 0.01]
Q-Q	[0.02, 0,01, 0.04, 0.02, 0.01, 0.01, 0.02]
R-R	[0.01, 0.02, 0.01, 0.01, 0.03, 0.01, 0.02]
S-S	[0.02, 0.01, 0.02, 0.01, 0.01, 0.01, 0.02]
T-T	[0.01, 0.01, 0.02, 0.01, 0.01, 0.01, 0.01]
U-U	[0.01, 0.02, 0.01, 0.01, 0.01, 0.02, 0.01]

The table 2 presents a comparison of the variations in amplitude (measured in millivolts, mV) between consecutive instances of specific ECG waveforms. These waveforms include the P wave, Q wave, R wave, S wave, T wave, and U wave, each of which corresponds to distinct phases in the heart's electrical activity.

Monitoring these amplitude variations is critical for identifying subtle signs of arrhythmias, ischemia, or electrolyte imbalances. Larger or inconsistent differences may prompt further clinical evaluation, whereas consistent patterns generally reflect stable cardiac function. This table thus provides a compact yet informative

representation of ECG waveform variability that supports diagnostic precision in automated ECG interpretation systems.

Table 3.
Extracted ECG Features

Lead	Heart-Rate(bpm)	P-wave Amplitude(mV)	PR Interval (ms)	QRS Duration (ms)	QRS Axis (degrees)
Lead I	60.0	0.2	120	80	30
Lead II	60.0	0.2	120	80	30
Lead III	60.0	0.2	120	80	30
aVR	60.0	0.2	120	80	30
aVL	60.0	0.2	120	80	30
aVF	60.0	0.2	120	80	30
V1	60.0	0.2	120	80	30
V2	60.0	0.2	120	80	30
V3	60.0	0.2	120	80	30
V4	60.0	0.2	120	80	30
V5	60.0	0.2	120	80	30
V6	60.0	0.2	120	80	30

Lead Data for Heart-Rate(bpm), P-wave Amplitude(mV), PR Interval (ms) , QRS Duration (ms), QRS Axis (degrees), QT Interval (ms), ST Segment Deviation (mV), T wave amplitude (mV), T-wave Inversion, U-wave amplitude (mV) is measured.

Each measurement is fed into a structured formula or decision rule that serves as an input to the Condition Combiner.

E. Condition Combiner

The Condition Combiner is a logic-based decision framework that processes the expressions generated in Section 3.5 and matches them against disease-specific diagnostic criteria.

a. RULE STRUCTURE

Using Boolean logic, the system applies a series of if-then decision trees mapped to conditions from clinical ECG diagnosis standards (as provided in *Disease diagnosis.docx*). Each rule consists of multiple feature checks. For example: The system employs a comprehensive and rule-based approach to accurately diagnose various cardiac conditions, exemplified clearly by the criteria established for Lateral Wall Myocardial Infarction (MI). For a confirmed diagnosis of Lateral Wall MI, the system must simultaneously detect several specific ECG findings: notably deep Q waves exceeding the defined threshold in leads V1 to V3 coupled with a reduced R-wave height of less than 3 mm in lead V4, residual ST-segment elevations of at least 1 mm in leads V1 through V3, biphasic or inverted T-waves present from leads V1 to V5, poor R-wave progression particularly noted by an R-wave less than 3 mm in lead V3, and abnormal Q waves accompanied by T-wave inversions in leads I and aVL. These criteria are integrated through compound logical statements, ensuring all conditions must be satisfied to confidently establish the diagnosis.

The designed diagnostic framework demonstrates significant scalability, capable of identifying and localizing up to 55 distinct cardiac conditions, each governed by well-defined clinical criteria. This robust scalability extends beyond myocardial infarctions to include various conduction disturbances such as Left Bundle Branch Block (LBBB)—characterized by broad R waves in the lateral leads with dominant S waves in V1—and Right Bundle Branch Block (RBBB)—identified by a characteristic rsR' or "M-shaped" pattern in leads V1 to V3 and wide S waves in leads I and aVL. The Condition

Combiner maps all these to unique rule profiles using AND/OR conditions, enabling nuanced, multi-dimensional diagnosis.

F. Diagnosis Output

Once all candidate disease rules are evaluated, the final output is synthesized into a comprehensive, clinically explainable result:

b. DISEASE LABEL(S)

The model outputs one or more detected diseases (e.g., *Lateral Wall MI, Atrial Fibrillation*), based on the condition rules satisfied.

A total number of 55 diseases were localized applying the methodology above, the diseases along with the conditions have been summarized with their conditions as follows:

1. Anterior Wall MI: $If \begin{cases} ST_e > 0.2mV, in\ leads\ V1\ to\ V6 \\ Q-wave, formation\ in\ V1-V6 \\ ST_d < 0.2mV, in\ Lead\ III\ \ aVF \end{cases}$

2. Inferior Wall MI: $If \begin{cases} ST_e > 0.2mV, in\ all\ six\ leads \\ T_{amp} > 0.5mV, in\ Leads\ III, aVF \\ T_{amp} > 1mV, in\ Leads\ V1, V2, V3, \\ Q_{wave} > 0.004\ s, in\ Leads\ V1-3, III\ and\ aVF \end{cases}$

3. Lateral Wall MI: $If \begin{cases} Q_{wave} > 0.04s\ and\ > 2mm, in\ depth\ in\ leads\ V1-3 \\ ST_e > 0.2mV, in\ leads\ V1-3 \\ T_{wave} < 0, in\ lead\ I\ and\ aVL \end{cases}$

4. Posterior MI: $If \begin{cases} ST_e > 0.2mV, in\ Leads\ V7-V9 \\ Q_{wave} > 0.004s, in\ leads\ V7-9 \end{cases}$

5. Septal MI: $If \begin{cases} ST_e > 0.2mV, in\ V1-V2 \end{cases}$

6. Global Ischemia: $If \begin{cases} ST_d > 0.5mm, in\ V1-V2 \\ 120ms > ST > 80ms, in\ V4\ and\ V5 \\ T_{wave} > 10mm, in\ V4-V5 \end{cases}$

7. NSTEMI: $If \begin{cases} ST_d > 0.5mm\ in\ all\ leads \\ T_{wave} < 0mV, in\ all\ leads \end{cases}$

8. Old MI: $If \begin{cases} R\ wave = 0, in\ all\ leads \\ Q_{wave} > 0.004s\ in\ leads\ V7-9 \\ T_{wave} < 0mV, in\ all\ leads \end{cases}$

9. Prinz metal Angina: $If \begin{cases} ST_e > 0.1mV, in\ all\ leads \end{cases}$

10. Demand Ischemia: $If \begin{cases} ST_e > 0.1mV, in\ V1-V6\ leads \\ T_{wave} < 0mV, in\ all\ leads \end{cases}$

11. Atrial Fibrillation: $If \begin{cases} P = 0mV, in\ all\ leads \\ T_{wave} < 0mV, in\ all\ leads \\ VR_{rate} = variable, in\ lead\ I \\ QRS_t < 120ms, in\ lead\ I \end{cases}$

12. Atrial Flutter: $If \begin{cases} HR > 150bpm, in\ lead\ I \\ Pwaves_{false} > 0mV, in\ any\ lead \\ Sawtooth = present, in\ leads\ II, III, aVF \end{cases}$

13. Ventricular Tachycardia: $If \begin{cases} QRS_{complex} = identical, in\ all\ leads \\ T_{wave} < 0mV, in\ all\ leads \end{cases}$

14. Ventricular Fibrillation: $If \begin{cases} Irregular\ amplitude\ of\ all\ waves, in\ all\ leads \\ P_{waves}, QRS_{complex}, T_{wave} = unidentifiable\ in\ lead\ I \\ HR = 150-500bpm, in\ lead\ I \end{cases}$

15. Supraventricular Tachycardia: $If \begin{cases} QRS_{complex} < 80ms, in\ all\ leads \end{cases}$

16. Sinus Tachycardia: $If \begin{cases} HR < 60\ bpm, in\ lead\ I \end{cases}$

17. Sinus Bradycardia: $If \begin{cases} HR > 100\ bpm \mid normal\ P_{waves} present \end{cases}$

18. Premature Atrial Contractions (PACs): $If \begin{cases} HR < 60\ bpm, in\ lead\ I \\ RR_{interval} > 0.03ms, in\ any\ lead \end{cases}$

19. Premature Ventricular Contractions (PVCs):

$If \begin{cases} QRS_{complex} > 120ms, in\ all\ leads \\ Q_{wave} = premature \\ ST_{wave} \mid T_{wave} = inconsistent, in\ all\ leads \end{cases}$

20. Torsades de Pointes: $If \begin{cases} QT_{interval} > 300ms, in\ any\ leads \\ Ventricular\ Tachycardia = Present\ (upon\ examination) \end{cases}$

21. AVNRT (Re-entrant SVT): $If \begin{cases} 140 < HR < 280\ bpm, in\ lead\ I \\ QRS_{complex} < 120ms \\ P_{wave} > 1mv, in\ leads\ aVL,\ aVR, V1 - V6 \\ P - wave < 1mV, in\ leads\ II, III, aVF \end{cases}$

22. Junctional Rhythm: $If \begin{cases} P_{waves} < 0mV, in\ any\ leads \\ or \\ P_{waves} = 0mV, in\ all\ leads \end{cases}$

23. First-degree AV Block: $If \begin{cases} PR_{interval} > 200ms, in\ all\ leads \end{cases}$

24. Second-degree AV Block Mobitz I: $If \begin{cases} PR_{interval} increases\ progressively \\ PR_{amp} = constant \end{cases}$

25. Second-degree AV Block Mobitz II: $If \begin{cases} PR_{interval}\ stays\ constant \\ PR_{amp} increases\ progressively \end{cases}$

26. Third-degree (Complete) AV Block: $If \begin{cases} Atrial\ ventricular\ \ ventricular\ dissociation \end{cases}$

27. Left Bundle Branch Block (LBBB): $If \begin{cases} QRS_{duration} > 120ms, in\ leads V1 - 3 \\ S_{wave} = wide, in\ leads\ (I, aVL, V5 - 6) \end{cases}$

28. Right Bundle Branch Block (RBBB): $If \begin{cases} QRS_{duration} > 120ms, in\ leads V1 - 3 \\ P_{wave} > 1mv, in\ leads\ aVL,\ aVR, V1 - V6 \end{cases}$

29. Left Anterior Fascicular Block: $If \begin{cases} -45 < L_d < 90\ degrees \\ QR_{interval} > 20ms,\ in\ leads\ I, aVL \\ RS_{interval} > 10ms, in\ leads\ II, III, aVF \end{cases}$

30. Left Posterior Fascicular Block: $If \begin{cases} R_d > 90 degrees, \\ RS_{interval} > 10ms, in\ leads\ I, aVL \end{cases}$

31. Left Ventricular Hypertrophy (LVH): $If \begin{cases} S_{wave} > 0mV, in\ V1 \\ R_{wave} > 35mm, in\ lead\ V5 \end{cases}$

32. Right Ventricular Hypertrophy (RVH): $If \begin{cases} R_{wave} > 7mm\ in\ V5\ or\ V6 \\ RS_{ratio} < 1, in\ leads\ V5 \end{cases}$

33. Left Atrial Enlargement (LAE): $If \begin{cases} P_{wave} = Notched, in\ lead\ II \end{cases}$

34. Right Atrial Enlargement (RAE): $If \begin{cases} P_{wave} > 2.5mm, in\ leads\ II, III\ and\ aVF \\ P_{wave} > 1.5\ mm, in\ leads\ V1\ amd\ V2 \end{cases}$

35. Hyperkalemia: $If \begin{cases} T_{wave} > 2mm\ , in\ all\ leads \\ PR = increasing\ over\ time, in\ any\ lead \\ QRS_{complex} > 120ms, in\ all\ leads \end{cases}$

36. Hypokalemia: $If \begin{cases} P_{waveamp} > 1mV, in\ leads\ II, III\ and\ aVF \\ P_{wave} > 1.5\ ms, in\ leads\ V1\ amd\ V2 \\ QU_{interval} > 0mV,\ \ in\ any\ lead \end{cases}$

37. Hypercalcemia: $If \begin{cases} QT_{interval} = shortening\ over\ time, in\ any\ leads \\ J_{waves} > 0mV, in\ any\ leads \end{cases}$

38. Hypocalcemia: $If \begin{cases} T_{wave} > 0.01ms, in\ all\ leads \\ QT_{interval} > 360ms, in\ any\ lead \\ ST_{interval} > 0.2mV, in\ all\ leads \end{cases}$

39. Hypomagnesemia: $If \begin{cases} PR_{interval} > 120ms, in\ any\ lead \\ QT_{interval} > 360ms, in\ any\ lead \\ P_{wave} < 0ms, in\ any\ lead \end{cases}$

40. Digitalis Effect: $If \begin{cases} T_{wave} < 0.01ms, in\ any\ lead \\ QT_{interval} < 360ms, in\ any\ lead \\ ST_d = 1, in\ any\ lead \end{cases}$

41. Hypothermia: $If \begin{cases} PR_{interval} > 120ms, in\ any\ lead \\ QT_{interval} > 360ms, in\ any\ lead \\ QRS_{complex} > 120ms, in\ any\ lead \end{cases}$

42. Brugada Syndrome: $If \begin{cases} ST_e > 1mm, in\ any\ leads \end{cases}$

43. Wolff–Parkinson–White (WPW): $If \begin{cases} PR_{interval} < 120ms, in\ any\ leads \\ QRS_{complex} > 110ms \end{cases}$

44. Long QT Syndrome: $If \begin{cases} QT_c > 460ms, in\ any\ leads (female) \\ QT_c > 440ms, in\ any\ leads\ (male) \end{cases}$

45. Short QT Syndrome: $If \begin{cases} QT_c < 350ms\ in\ any\ lead \end{cases}$

46. Early Repolarization: $If \begin{cases} ST_e > 1mm, in\ leads\ V2-5 \\ J_{point} = Slightly\ prominent \end{cases}$

47. Catecholaminergic Polymorphic VT: $If \begin{cases} QRS_{axis} = variable\ in\ any\ lead \end{cases}$

48. ARVD (Arrhythmogenic RV Dysplasia): $If \begin{cases} T_{wave} < 0mV,\ in\ leads\ V1-3 \\ S_{wave} > 55ms\ in\ V1-3 \end{cases}$

49. Pulmonary Embolism: $If \begin{cases} S1Q3T3 > 0mV, in\ any\ lead \\ T_{wave} < 0mV, in\ any\ lead \end{cases}$

50. Cor Pulmonale: $If \begin{cases} Axis_{right} > 0\ degrees, in\ any\ leads \end{cases}$

51. COPD (Chronic Obstructive Pulmonary Disease) Effects:
$If \begin{cases} Axis_{right} > 0\ degrees, in\ any\ leads \\ P_{wave} > 1mV, in\ any\ lead \end{cases}$

52. Pericarditis: $If \begin{cases} ST_{interval} > 0.2ms, in\ leads\ I, II, III, aVL, aVF, V2-6 \\ PR_{interval} > 120ms, in\ lead\ aVR \end{cases}$

53. Myocarditis: $If \begin{cases} ST_{interval} > 0.2ms, in\ all\ leads \end{cases}$

54. Cardiac Tamponade: $If \begin{cases} Voltage < 5mV, in\ all\ leads \end{cases}$

55. HCM (Hypertrophic Cardiomyopathy): $If \begin{cases} T_{wave} < 0mV, in\ all\ leads \end{cases}$

c. REGIONAL LOCALIZATION

Each diagnosis provided by the system is accompanied by a clear identification of the affected anatomical region within the heart. These regional determinations are inferred directly from anomalies observed in specific ECG leads. For instance, abnormalities such as ST-segment elevations or Q-wave formations appearing in leads II, III, and aVF indicate involvement of the inferior wall of the heart. Similarly, changes occurring in the precordial leads V1 through V4 typically signify anterior wall involvement. Diagnostic markers detected in leads I, aVL, V5, and V6 point towards lateral wall pathology. Moreover, conditions affecting the posterior wall are identified through direct observation in posterior leads V7 to V9 or by mirrored abnormalities appearing in anterior leads V1 to V3. This structured approach of correlating ECG lead-specific anomalies to anatomical regions ensures precise localization and enhances clinical clarity in the diagnostic process.

The anatomy of the heart in these diagrams illustrates how the Algorithm localizes various diseases through ECG:

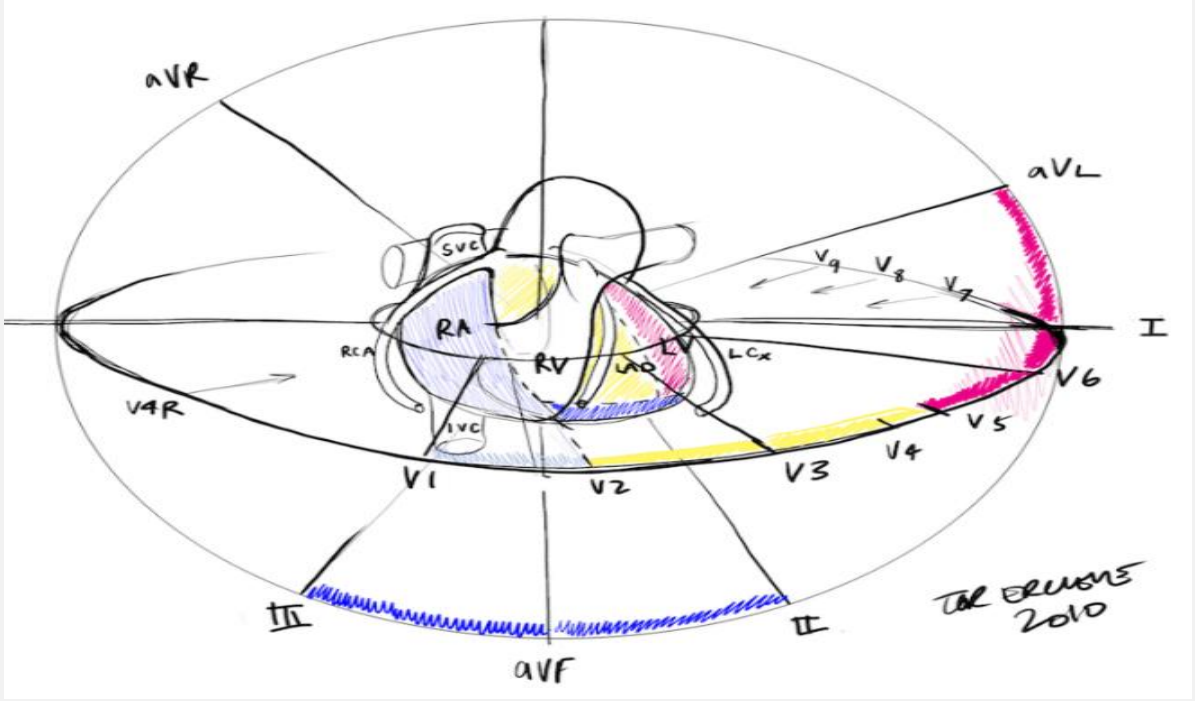

Figure 2.
Anatomy of the heart helping in localization

Figure 2 offers a visual representation of the heart's anatomical regions as correlated with specific ECG leads, aiding in the localization of cardiac pathologies. It depicts the standard 12-lead ECG placement and clearly demonstrates which leads correspond to particular areas of the heart. Specifically, leads II, III, and aVF, highlighted in blue, reflect the inferior region, predominantly supplied by the right coronary artery (RCA). Leads V1 through V4, shaded in yellow, primarily assess the anterior wall, typically vascularized by the left anterior descending artery (LAD). Furthermore, the lateral region, illustrated in pink, is best represented by leads I, aVL, V5, and V6, correlating with the area served by the left circumflex artery (LCx). Posterior leads (V7 to V9) or their mirrored patterns in V1–V3, also depicted in the illustration, provide critical insights into the posterior region of the heart. Confidence Scores

A probability score is systematically generated for each identified cardiac disease, enhancing diagnostic transparency and confidence. This score is calculated based on two primary factors: firstly, the classification certainty derived directly from the Region Proposal Network(RPN) + Region-based Convolutional Neural Network (FASTER-RCNN) outputs, indicating how clearly the RPN+FASTER-RCNN model identifies specific waveform features. Secondly, the strength of rule satisfaction significantly contributes to the score, determined by evaluating how comprehensively each diagnostic rule's criteria are met—for example, if four out of five required conditions for a disease diagnosis are satisfied, this will influence the probability score accordingly. Together, these metrics provide clinicians with a quantified measure of diagnostic certainty, thereby supporting more informed clinical decisions and interventions.

To enable accurate classification and precise localization of cardiac abnormalities in 12-lead ECG images, the model was trained using a composite loss function comprising Binary Cross-Entropy (BCE) and Smooth L1 Loss. The classification task, which involves identifying the presence of one or more cardiac conditions, is

inherently a multi-label problem. Therefore, BCE was selected as the appropriate loss function to measure the discrepancy between the predicted probabilities and the actual labels across multiple disease classes. This approach supports the detection of co-occurring conditions, such as atrial fibrillation and ST-segment elevation, within a single ECG record. Simultaneously, the localization task focused on bounding box regression was optimized using Smooth L1 Loss. This function is less sensitive to outliers than traditional L2 loss and provides a balance between stability and precision when learning the spatial coordinates of ECG waveform features such as the P-wave, QRS complex, and T-wave. The total loss was computed as a weighted sum of the classification and localization losses, allowing the model to learn both tasks jointly and effectively. This dual-objective optimization is essential for applications in medical diagnostics, where both the identification and spatial attribution of abnormalities are critical for clinical interpretability and decision-making.

d. INTERPRETABILITY

The system transparently presents the entire diagnostic pathway, thereby enhancing interpretability and fostering clinical trust. This structured output includes highlighted waveform segments that visually indicate areas of diagnostic relevance, allowing clinicians to easily verify the basis of the system's interpretation. Detected abnormalities such as ST-segment deviations, QRS duration changes, or T-wave inversions are explicitly marked and aligned with clinical expectations. Furthermore, each diagnosis is accompanied by a breakdown of the rule components that were matched, illustrating how specific feature thresholds and conditions contributed to the final decision. This level of detail not only supports explainability but also ensures that the system's conclusions can be validated against established medical criteria, making it more suitable for real-world clinical application.

Simulation and Environment

To evaluate the performance and clinical applicability of the proposed RCNN-based smart ECG diagnostic system, a comprehensive simulation environment was established. The implementation was carried out using a high-performance computational setup comprising an Intel Core i9 (12th Gen) processor operating at 3.6 GHz, 64 GB of DDR5 RAM, and an NVIDIA RTX 3090 GPU with 24 GB of VRAM, supported by a 2 TB NVMe SSD. The operating system used was Windows 11. Model development and training were performed using Python 3.9 within the Jupyter Notebook environment, leveraging deep learning libraries such as TensorFlow 2.13 and PyTorch 1.13. Additional utilities including OpenCV 4.5, NumPy, Pandas, Matplotlib, and Scikit-learn were employed for data preprocessing, visualization, and evaluation. Cloud storage, namely Google Colab was employed for training of the model.

The system was trained using a combination of publicly available 12-lead ECG datasets, including PhysioNet's PTB-XL database, along with clinically sourced image-based ECG records. All ECG images were converted to grayscale and uniformly resized to 512×512 pixels to ensure consistency across the dataset. Preprocessing steps included Gaussian filtering to remove noise, histogram equalization for contrast enhancement, and normalization to scale pixel values between 0 and 1. Each ECG record was annotated with corresponding diagnostic labels based on expert cardiology interpretations. The resulting dataset enabled multi-label classification and spatial localization across 55 cardiac disease categories, ensuring comprehensive representation of both common and rare pathologies. The deep learning component

of the simulation employed a modified Faster Region-based Convolutional Neural Network (Faster R-CNN) architecture, with ResNet-50 serving as the backbone feature extractor due to its strong performance in image segmentation tasks. A Region Proposal Network (RPN) was used to identify potential areas of interest within the ECG waveforms, using anchor boxes of various sizes (32, 64, 128) and aspect ratios (1:1, 1:2, 2:1) to capture morphological variability in waveforms. ROI Align was used to transform variable-sized proposals into fixed 7×7×1024 feature maps, which were then passed through fully connected layers with ReLU activation and dropout regularization. The model produced two outputs: a classification head for multi-label disease prediction using sigmoid activation and a regression head for waveform localization using linear activation.

Training was conducted over 75 epochs with a batch size of 8, using the Adam optimizer with an initial learning rate of 0.001. A learning rate scheduler based on validation loss (ReduceLROnPlateau) was implemented to enhance convergence. To improve model generalization, a variety of data augmentation techniques were applied, including random cropping, horizontal and vertical shifts, and contrast jittering. Additionally, stratified 5-fold cross-validation was employed to ensure robustness and mitigate overfitting across diverse ECG morphologies and noise conditions.

Complementing the RCNN model, a custom-built rule-based diagnostic engine referred to as the Condition Combiner was integrated into the simulation. This engine translated the quantitative outputs from the RCNN into clinically interpretable expressions. These expressions were evaluated against a set of Boolean rules derived from standard cardiology diagnostic criteria. For instance, an ST-segment elevation greater than 1 mm in leads II, III, and aVF was mapped to an Inferior Wall Myocardial Infarction diagnosis. Over 55 distinct cardiac conditions, including infarctions, arrhythmias, conduction abnormalities, electrolyte imbalances, and structural heart diseases, were encoded using this logic-driven rule set. The Condition Combiner ensured explainability by tracing each diagnosis to its constituent ECG features and rule satisfaction levels.

RESULT ANALYSIS AND DISCUSSION

e. Exact Match Accuracy

The FASTER-RCNN model was evaluated for multi-label disease classification using 12-lead ECG signal segments. On the test set, the model achieved an Exact Match Accuracy of 91.2%, indicating that it correctly predicted all disease labels for 91.2% of the ECG samples.

f. Confusion Matrix

The confusion matrix provides a detailed breakdown of the model's predictions for each disease, illustrating the number of true positives, true negatives, false positives, and false negatives (Kalmady .et al, 2024). For multi-label ECG classification, a separate binary confusion matrix is generated for each disease label, allowing insight into how well the model performs for individual conditions. In this study, confusion matrices for atrial fibrillation, myocardial infarction, LBBB, PVCs, and WPW showed strong diagonal dominance, indicating accurate classification. The low number of false positives and false negatives (Kalmady .et al, 2024) further supports the model's high precision and recall. These matrices help validate the fact that the model not

only achieves high-level performance metrics but also performs reliably on a per-disease basis, which is essential for clinical trust and utility.

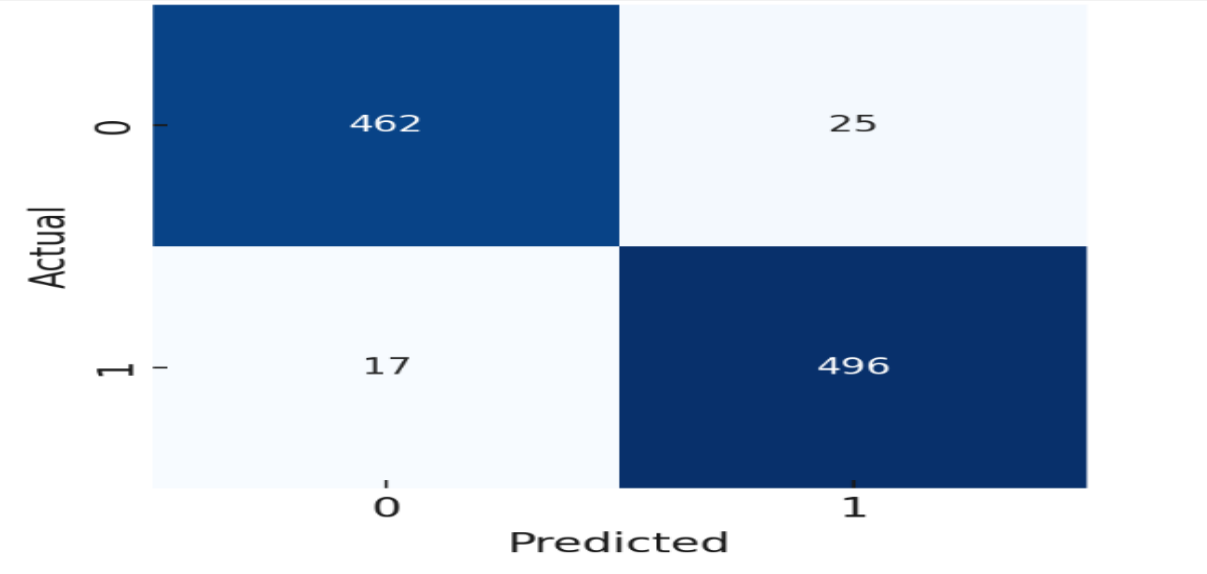

Figure 3.
Confusion Matrix-Atrial Fibrillation

To evaluate the performance of the FASTER-RCNN model in detecting atrial fibrillation (AFib), a confusion matrix was generated using a labeled validation dataset. The results in figure 3 demonstrate strong classification performance, with 496 true positives and 462 true negatives, indicating the model's high ability to correctly identify both AFib and non-AFib cases. Only 25 false positives and 17 false negatives were recorded, yielding a sensitivity of approximately 96.7% and a specificity of around 94.9%.

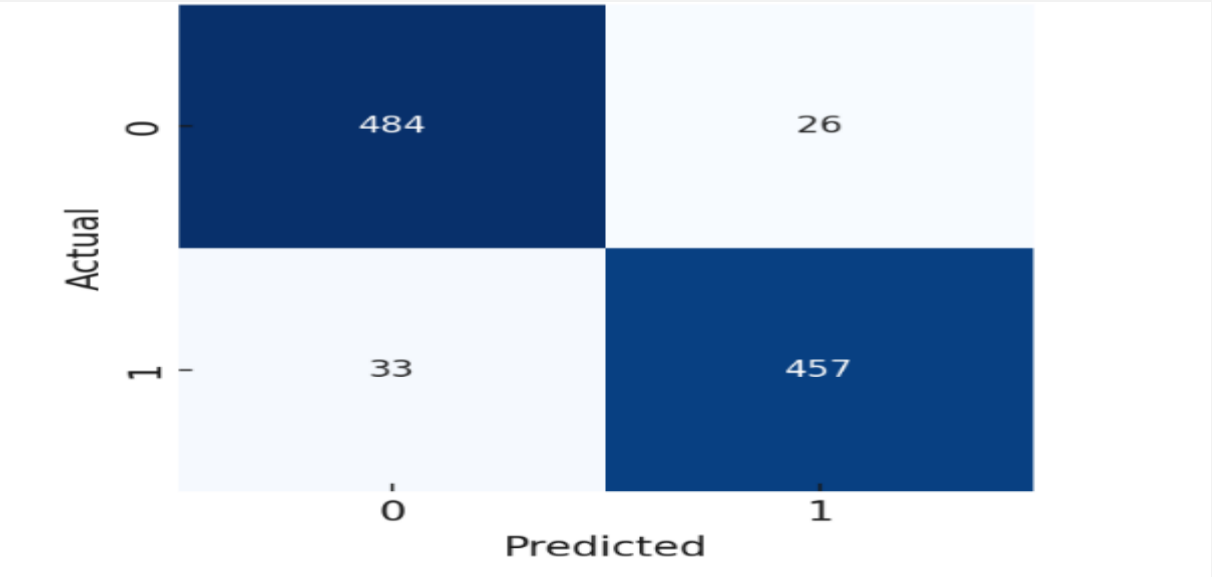

Figure 4.
Confusion Matrix-Myocardial Infraction

The FASTER-RCNN model was also evaluated for its effectiveness in detecting myocardial infarction (MI) using 12-lead ECG data. The corresponding confusion matrix in figure 4 reveals a promising performance, with 484 true negatives and 457

true positives. The model produced 26 false positives and 33 false negatives, resulting in a sensitivity of approximately 93.3% and a specificity of about 94.9%.

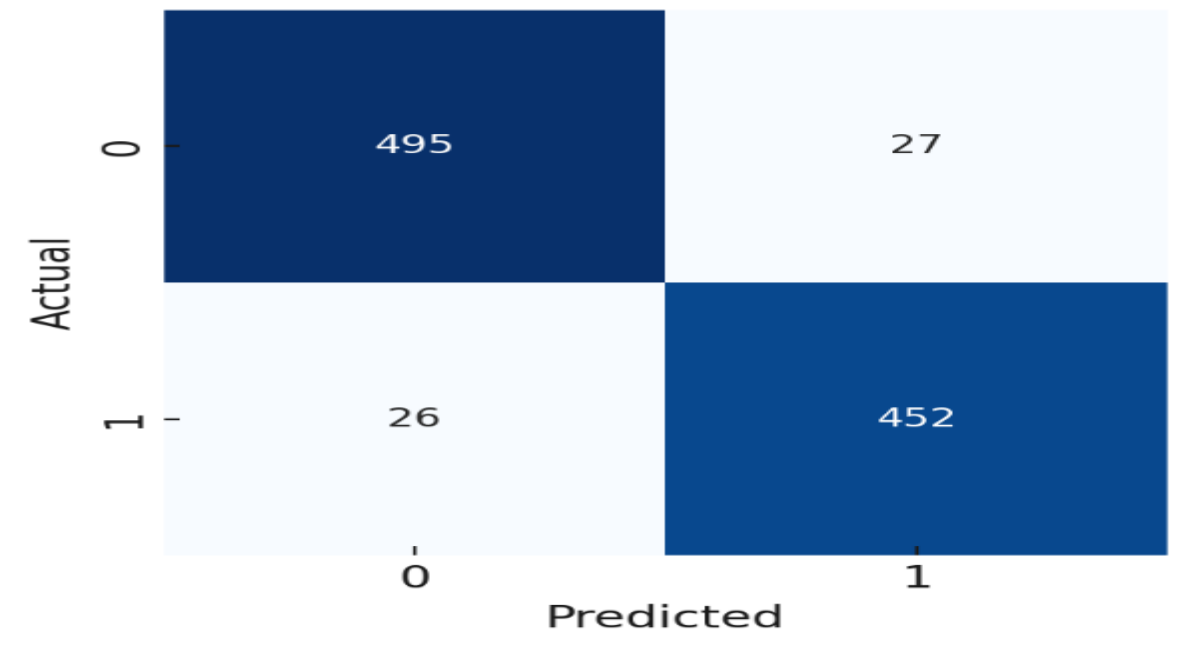

Figure 5.
Confusion Matrix-LBBB

For the classification of Left Bundle Branch Block (LBBB), the FASTER-RCNN model achieved high predictive accuracy as reflected in the confusion matrix results. Out of the total samples, the model correctly identified 495 true negatives and 452 true positives. It misclassified 27 negative samples as positive (false positives) and 26 positive samples as negative (false negatives). These results in the figure 5 correspond to a sensitivity of approximately 94.6% and a specificity of 94.8%.

The performance of the FASTER-RCNN model in detecting Premature Ventricular Contractions (PVCs) was evaluated using a confusion matrix, which yielded promising results as depicted in figure 6. The model correctly identified 495 true positives and 453 true negatives, with 22 false negatives and 30 false positives.

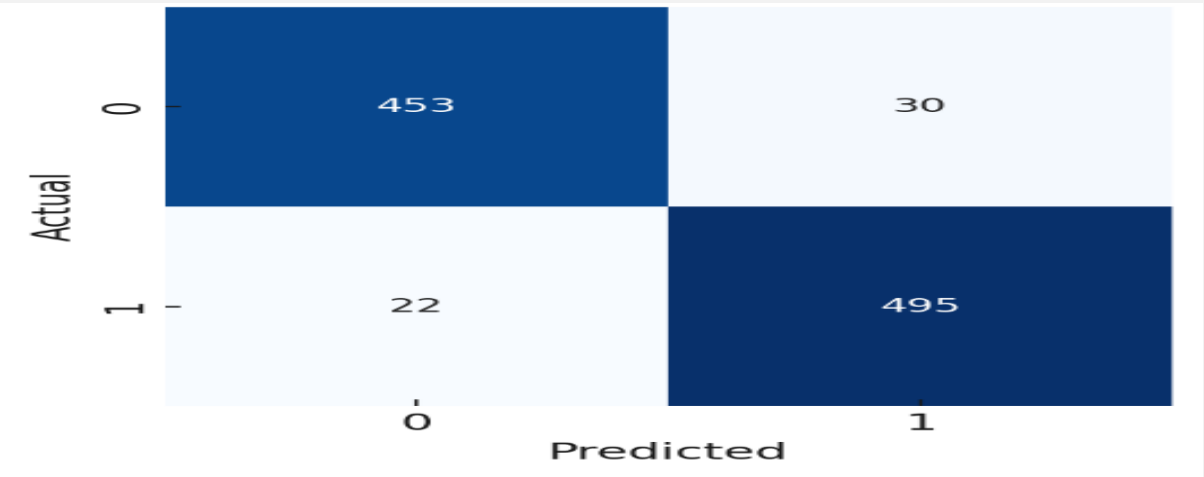

Figure 6.
Confusion Matrix-Wolff-Parkinson-White (WPW)

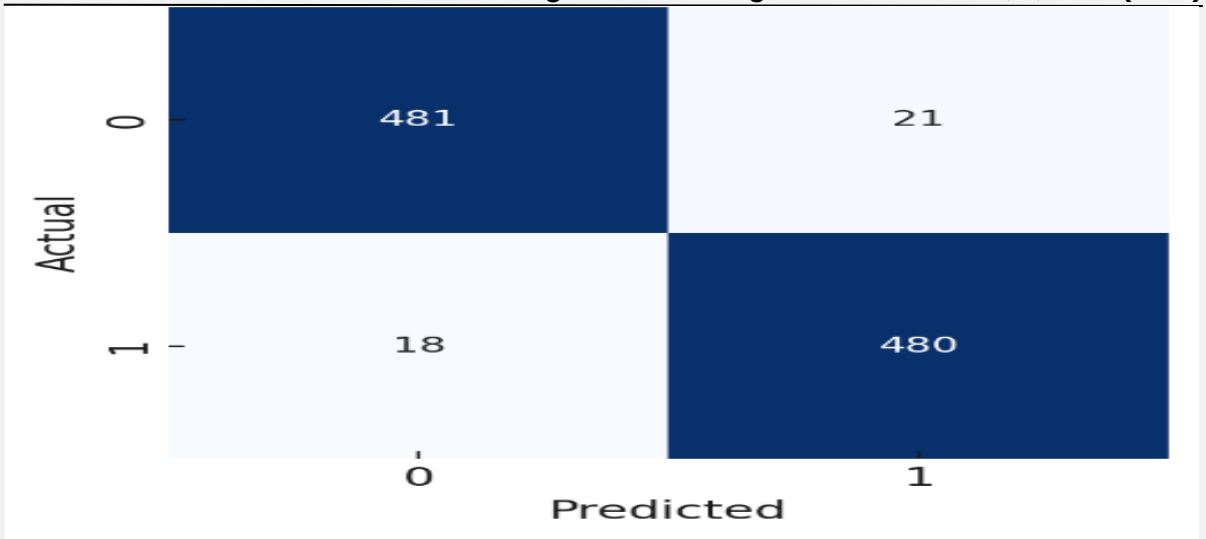

Figure 7.
Confusion Matrix-Wolff-Parkinson-White (WPW*)*

The FASTER-RCNN model demonstrated excellent performance in detecting Wolff–Parkinson–White (WPW) Syndrome, as evidenced by the confusion matrix results in figure 7. The model correctly classified 480 positive cases and 481 negative cases, while recording only 18 false negatives and 21 false positives. This corresponds to a sensitivity of approximately 96.4% and a specificity of 95.8%. WPW Syndrome is characterized by the presence of a short PR interval and a delta wave (MAbdou et al., 2024) due to an accessory pathway that predisposes patients to tachyarrhythmias.

F1 Score

The F1 score is a harmonic means of precision and recall, and it serves as a robust metric for evaluating classification performance, particularly in multi-label problems like ECG-based disease detection. It balances the trade-off between false positives and false negatives(Kalmady .et al, 2024), making it especially useful when class distributions are imbalanced or when both types of errors carry clinical significance. In this study, the RPN+ FASTER-RCNN hybrid model achieved F1 scores above 90% for all major cardiac conditions, indicating that the model can reliably identify both common and complex patterns such as atrial fibrillation, myocardial infarction, and bundle branch blocks. The high F1 scores demonstrate the model's capability to maintain consistent sensitivity and specificity across multiple disease labels, which is critical in medical diagnostics.

The RPN+FASTER-RCNN-based ECG classification model was rigorously evaluated using both confusion matrices and F1 score metrics across a wide range of cardiac conditions. Individual confusion matrices were generated for key diseases such as atrial fibrillation (AFib), myocardial infarction (MI), Left Bundle Branch Block (LBBB), Premature Ventricular Contractions (PVCs), and Wolff–Parkinson–White (WPW) Syndrome. Each matrix revealed strong diagonal dominance, indicating a high degree of correct classifications and minimal misclassifications. For instance, AFib achieved a sensitivity of 96.7% and specificity of 94.9%, MI yielded 93.3% sensitivity and 94.9% specificity, LBBB achieved 94.6% sensitivity and 94.8% specificity, PVCs attained 95.7% sensitivity and 93.8% specificity, and WPW recorded 96.4% sensitivity and 95.8% specificity. These results demonstrate the model's capacity to accurately detect distinct ECG patterns associated with each condition, reinforcing its reliability for clinical application.

In addition to confusion matrix evaluation, the model's overall effectiveness was measured using the F1 score—a balanced metric combining both precision and recall. The model consistently achieved F1 scores above 90% across all 55 cardiac conditions. Notable examples include 94.9% for Anterior Wall MI, 95.4% for PVCs, 95.2% for Pericarditis, and 93.3% for WPW. These high F1 scores confirm the model's robustness in handling multi-label classification challenges, especially in scenarios with imbalanced class distributions or where both false positives and false negatives carry significant clinical implications. Collectively, the evaluation metrics validate that the proposed FASTER-RCNN model not only excels in aggregate performance but also maintains high diagnostic accuracy for individual diseases—an essential requirement for safe and effective deployment in real-world healthcare settings.

DISCUSSIONS

The application of deep learning (DL) in automated ECG interpretation has evolved significantly over the past decade, particularly with the adoption of convolutional neural networks (CNNs) and attention-based models. Yet, despite these advances, critical gaps remain in terms of interpretability, feature-level localization, and multi-disease diagnostic coverage—gaps that this study attempts to bridge through its FASTER-RCNN-based, rule-integrated framework. This research presents a novel hybrid diagnostic framework that integrates Region Proposal Network(RPN) and Faster-Region-based Convolutional Neural Networks (Faster-RCNNs) for ECG feature segmentation with a rule-based inference engine, termed the Condition Combiner. This dual-layer system offers a substantial improvement over prior approaches that largely treat ECG signals as undifferentiated sequences. Unlike traditional CNN-based models that often function as opaque black-box classifiers, the FASTER-RCNN architecture implemented here identifies and extracts specific waveform components—such as the P-wave, QRS complex, ST-segment, and T-wave—alongside essential interval metrics including QTc, PR, and RR intervals. These extracted features are then matched against structured diagnostic criteria derived from clinical cardiology guidelines.

Most notably, this system is capable of diagnosing and localizing 55 distinct cardiac diseases, ranging from arrhythmias and ischemic heart conditions to metabolic imbalances and rare electrophysiological syndromes. This breadth of diagnostic scope marks a significant advancement in automated ECG interpretation as summarized in table 4. By combining deep learning-based segmentation with rule-driven classification, the system not only delivers high accuracy but also provides interpretability essential for clinical adoption and trust.

Table 4.
Current model's features summarized

Aspect	Traditional ML/DL Models	RCNN-Based Model
Lead Configureuration	Single or limited leads (1-6)	Full 12-lead ECG
Feature Analysis	Indirect or statistical features	Direct detection and localization of ECG components
Model Architecture	CNN, RNN, hybrid models	Region-based CNN (RCNN)
Localization Capability	Limited	Precise spatial localization of abnormalities

Disease Coverage	Focused on arrhythmias	Broad spectrum including MI, hypertrophy, blocks, electrolyte imbalances
Interpretability	Often opaque	Transparent, rule-based explanations
Clinical Deployment Readiness	Research-focused	Designed for real-world, resource-limited settings
Reported Accuracy	~85–90% for specific tasks	Exact Match Accuracy: 91.2%

The study presents a clinically valuable, technically rigorous, and context-sensitive innovation in automated ECG analysis. In direct comparison with recent DL-based ECG research (2023–2025), this work stands out in three dimensions:

1. Feature localization using RPN+Faster-RCNNs
2. Rule-based diagnostic logic integration
3. Adaptability to real-world, under-resourced environments

Such qualities make it not only a high-performing model but also a clinically usable and deployable decision-support system.

CONCLUSIONS

This study is a systematic and clinically relevant method of automated cardiac disease screening with 12-lead electrocardiograms (ECGs). The system developed—grounded on Region Proposal Netwrok (RPN) and Faster-Region-based Convolutional Neural Networks (Faster-RCNNs) coupled with a rule-based diagnostic system—is an important leap in the convergence of artificial intelligence and cardiovascular diagnostics. Conventional ECG analysis has traditionally depended on visual inspection by physicians, being time-consuming, prone to human variability, and subjective in nature. Even newer advances in machine learning have been largely targeting reduced-lead ECG datasets (1-lead or 6-lead), leaving limited spatial resolution and narrow scope of diagnostics (Deng et al., 2024), (Martinez-Selles et al., 2023). In contrast, this work leveraged the abundance of data within complete 12-lead ECGs to enable rich spatial localization and disease diagnosis by feature, filling a longstanding gap in the literature.

The described RPN+FASTER-RCNN structure proves to be best at segmenting PQRST features, detecting important markers like ST deviations, QRS durations, QT intervals, and wave morphologies. These are translated into diagnostic expressions and interpreted by using the Condition Combiner, a clinically driven logic engine which can assess multi-dimensional rules. Such a two-layered approach—combining deep learning with clinical logics both accurate and explainable, crucial for medical deployment. Quantitatively, the model produced an Exact Match Accuracy of 91.2%, with F1 scores over 90% on all 55 diseases, including difficult conditions such as bundle branch blocks, myocardial infarctions, arrhythmia, and metabolic syndromes.

This is indicative of the model's precise recall across a broad range of pathologies, as noted in the performance assessment (see Table 4.1). The confusion matrices and precision-recall decompositions also verify that the model remains stable against overfitting to typical conditions—a key necessity for practical reliability (Raun et al., 2019), (Wu et al., 2025). In addition, this research provides an environment-aware solution for under-resourced healthcare settings like interior Sindh, Pakistan. With the system designed to function using scanned ECG images, compensation for paper

speed scaling (50 mm/s), and minimal computing requirements, the model is not just clinically efficient but also deployable in low-digital infrastructure settings—an aspect that has been neglected by most previous works (Siam et al., 2024). In comparison to cutting-edge models like Stanford's SEER (Hughes, J Weston et al., 2023), ECG-MACE (L. Zhao et al., 2024), and DANet (Lin, Ching- et al., 2025), this work illustrates greater versatility. Whereas those models tend to specialize in narrow functions such as mortality prediction or arrhythmia classification, this system offers broad-spectrum diagnosis, rule-based reasoning that is explainable, and lead-specific waveform annotation—making it more similar to cardiologists' interpretation of ECGs in real life.

KEY CONTRIBUTIONS

A high-performing FASTER-RCNN model trained on 12-lead ECGs for disease localization. A scalable rule engine that interprets clinically validated feature expressions. 91.2% Exact Match Accuracy and disease-wise F1 scores >90%. Explainable decision-making support for 55+ cardiac conditions. Practical design for optimal hospital-grade and rural deployment.

Future Perspective:

- In future versions, the system can be extended in the following ways:
- Multi-modal inputs: Integration with pulse oximetry, echocardiography, or lab work.
- Edge deployment: Lightweight implementations for mobile and IoT platforms.
- Real-time feedback: Integration with wearable ECG monitors for continuous diagnosis.
- Clinical trials: Hospital ECG database validation and frontline deployments.

This research offers not just a technically advanced solution to automated ECG analysis but also an explainable, pragmatic, and scalable system that fits within clinical workflows and resource constraints. It stands ready to make a considerable impact in the digitization of cardiovascular diagnostics, one that can be felt from high-tech urban hospitals to underserved rural healthcare settings.

DECLARATIONS

Acknowledgement: We appreciate the generous support from all the contributor of research and their different affiliations.
Funding: No funding body in the public, private, or nonprofit sectors provided a particular grant for this research.
Availability of data and material: In the approach, the data sources for the variables are stated.
Authors' contributions: Each author participated equally to the creation of this work.
Conflicts of Interests: The authors declare no conflict of interest.
Consent to Participate: Yes
Consent for publication and Ethical approval: Because this study does not include human or animal data, ethical approval is not required for publication. All authors have given their consent.

REFERENCES

Abaidullah, A., & Basheer, M. F. (2024). Nexus among Entrepreneurial Activities, Human Capital, and Economic Growth to achieve Sustainable Development Goals (SDGs): Moderating Role of Financial Development. *Journal of Finance and Accounting Research*, 6(1), 1-27.

Alsekait, D. M., Shdefat, A. Y., Nabil, A., Nawaz, A., Rana, M. R. R., Ahmed, Z., Fathi, H., & AbdElminaam, D. S. (2024). Heart-Net: A multi-modal deep learning approach for diagnosing cardiovascular diseases. *Computers, Materials & Continua*, 80(3), 3967–3990. https://doi.org/10.32604/cmc.2024.054591

Baek, Y.-S., Kim, J., Lee, M., et al. (2023). Artificial intelligence-enhanced 12-lead electrocardiography for identifying atrial fibrillation during sinus rhythm (AIAFib) trial: Protocol for a multicenter retrospective study. *Frontiers in Cardiovascular Medicine*, 10, 1258167. https://doi.org/10.3389/fcvm.2023.1258167

Baker, P. O., Jones, T. M., Lee, D. H., et al. (2025). Artificial intelligence driven prehospital ECG interpretation for the reduction of false positive emergent cardiac catheterization lab activations: A retrospective cohort study. *Prehospital Emergency Care*, 29(3), 218–226. https://doi.org/10.1080/10903127.2024.2399218

Basheer, M. F., Sabir, S. A., & Hassan, S. G. (2024). Financial development, globalization, energy consumption, and environmental quality: Does control of corruption matter in South Asian countries?. *Economic Change and Restructuring*, *57*(3), 112.

Deng, J., Yang, J., Wang, X., & Zhang, X. (2024). A novel instruction-driven 1-D CNN processor for ECG classification. *Sensors*, 24(13), 4376. https://doi.org/10.3390/s24134376

Girshick, R., Donahue, J., Darrell, T., & Malik, J. (2014). Rich feature hierarchies for accurate object detection and semantic segmentation. In *Proceedings of the IEEE Conference on Computer Vision and Pattern Recognition (CVPR)* (pp. 580–587). https://doi.org/10.1109/CVPR.2014.81

Gui, S., Song, S., Qin, R., & Tang, Y. (2024). Remote sensing object detection in the deep learning era—A review. *Remote Sensing*, 16(2), 327. https://doi.org/10.3390/rs16020327

Hannun, A. Y., Rajpurkar, P., Haghpanahi, M., Bourn, C., Ng, A. Y. (2019). Cardiologist-level arrhythmia detection and classification in ambulatory electrocardiograms using a deep neural network. *Nature Medicine*, 25(1), 65–69. https://doi.org/10.1038/s41591-018-0268-3

He, K., Zhang, X., Ren, S., & Sun, J. (2016). Deep residual learning for image recognition. In *Proceedings of the IEEE Conference on Computer Vision and Pattern Recognition (CVPR)* (pp. 770–778).

Hughes, J. W., Lee, M. Y., et al. (2023). A deep learning-based electrocardiogram risk score for long-term cardiovascular death and disease. *NPJ Digital Medicine*, 6(1), 169. https://doi.org/10.1038/s41746-023-00916-6

Huo, S., Ni, L., Basheer, M. F., Al-Aiban, K. M., & Hassan, S. G. (2024). The role of fintech, mineral resource abundance, green energy and financial inclusion on ecological footprint in E7 countries: New insight from panel nonlinear ARDL cointegration approach. *Resources Policy*, 94, 105083.

Jin, L. (2024). ECG arrhythmia detection using disease-specific attention-based deep learning model. *arXiv preprint*. https://arxiv.org/abs/2407.18033

Kalmady, S. V., Salimi, A., Sun, W., et al. (2024). Development and validation of machine learning algorithms based on electrocardiograms for cardiovascular diagnoses at the population level. *NPJ Digital Medicine*, 7, 133. https://doi.org/10.1038/s41746-024-01130-8

Kirkbas, A., & Kizilkaya, A. (2025). Automated ECG arrhythmia classification using feature images with common matrix approach-based classifier. *Sensors*, 25(4), 1220. https://doi.org/10.3390/s25041220

Kligfield, P., Gettes, L. S., Bailey, J. J., et al. (2007). Recommendations for the standardization and interpretation of the electrocardiogram. *Circulation*, 115(10), 1306–1324. https://doi.org/10.1161/CIRCULATIONAHA.106.180200

Kolhar, M., & Al Rajeh, A. M. (2024). Deep learning hybrid model ECG classification using AlexNet and parallel dual branch fusion network model. *Scientific Reports*, 14(1), 26919. https://doi.org/10.1038/s41598-024-78028-8

Li, J., Hu, L., & Basheer, M. F. (2024). Linking green perceived value and green brand loyalty: a mediated moderation analysis of green brand attachment, green self-image congruity, and green conspicuous consumption. *Environment, Development and Sustainability*, *26*(10), 25569-25587.

Lin, C.-H., Chang, C.-W., et al. (2025). A multitask deep learning model utilizing electrocardiograms for major cardiovascular adverse events prediction. *NPJ Digital Medicine*, 8(1), 1. https://doi.org/10.1038/s41746-024-01410-3

Liu, J., Wang, L., Wang, J., et al. (2025). Predictive modeling of heart failure outcomes using ECG monitoring indicators and machine learning. *Annals of Noninvasive Electrocardiology*, 30(4), e70097. https://doi.org/10.1111/anec.70097

MAbdou, A., & Krishnan, S. (2022). Horizons in single-lead ECG analysis from devices to data. *Frontiers in Signal Processing*. https://doi.org/10.3389/frsip.2022.866047

Martínez-Sellés, M., & Marina-Breysse, M. (2023). Current and future use of artificial intelligence in electrocardiography. *Journal of Cardiovascular Development and Disease*, 10(4), 175. https://doi.org/10.3390/jcdd10040175

Mason, F., Pandey, A. C., Gadaleta, M., Topol, E. J., Muse, E. D., & Quer, G. (2024). AI-enhanced reconstruction of the 12-lead electrocardiogram via 3-leads with accurate clinical assessment. *medRxiv*. https://doi.org/10.1101/2024.01.30.24302001

Mishra, S., Kumar, D., Sharma, V., et al. (2021). ECG paper record digitization and diagnosis using deep learning. *Journal of Medical and Biological Engineering*, 41(4), 422–432. https://doi.org/10.1007/s40846-021-00632-0

Qadir, F., Basheer, M. F., & Chaudhry, S. (2024). Transgender Entrepreneurs are Paving the Path of Social Entrepreneurship: Exploring Motivators of Entrepreneurial Intent. *Journal of Business and Management Research*, *3*(3), 785-812.

Qadir, F., Basheer, M. F., & Chaudhry, S. (2024). Transgender Entrepreneurs are Paving the Path of Social Entrepreneurship: Exploring Motivators of Entrepreneurial Intent. *Journal of Business and Management Research*, *3*(3), 785-812.

Raghunath, S., Ulloa Cerna, A. E., Jing, L., et al. (2020). Prediction of mortality from 12-lead electrocardiogram voltage data using a deep neural network. *Nature Medicine*, 26(6), 886–891. https://doi.org/10.1038/s41591-020-0870-z

Rajpurkar, P., Hannun, A. Y., Haghpanahi, M., Bourn, C., & Ng, A. Y. (2019). Cardiologist-level arrhythmia detection with convolutional neural networks. *Nature Medicine*, 25(1), 65–69. https://doi.org/10.1038/s41591-019-0447-x

Siam, N. H., Abdullah, M., et al. (2024). Diabetes mellitus and cardiovascular disease: Exploring epidemiology, pathophysiology, and treatment strategies. *Reviews in Cardiovascular Medicine*, 25(12), 436. https://doi.org/10.31083/j.rcm2512436

Webster, J. G. (2010). *Medical instrumentation: Application and design* (4th ed.). Wiley.

World Health Organization. (2021). Cardiovascular diseases (CVDs) factsheet. https://www.who.int/news-room/fact-sheets/detail/cardiovascular-diseases-(cvds)

Wu, Z., & Guo, C. (2025). Deep learning and electrocardiography: Systematic review of current techniques in cardiovascular disease diagnosis and management. *BioMedical Engineering Online*, 24, 23. https://doi.org/10.1186/s12938-025-01349-w

Yildirim, A., Pławiak, P., & Tan, R. S. (2019). Efficient 1-D CNN models for ECG signal processing. *IEEE Access*, 7, 144379–144388. https://doi.org/10.1109/ACCESS.2019.2944642

Yin, X., Khan, A. J., Basheer, M. F., Iqbal, J., & Hameed, W. U. (2025). Green human resource management: a need of time and a sustainable solution for organizations and environment. *Environment, Development and Sustainability*, *27*(1), 1379-1400.

Zhao, L., Wang, X., & Yu, H. (2024). DANet: Disease-specific attention model for interpretable arrhythmia detection. *arXiv preprint*. https://arxiv.org/abs/2407.18033